VERTICALLY PROPAGATING SEICHES AND STANDING MODES PRECLUSION IN A STEEP-BOTTOM TROPICAL RESERVOIR

Andrés Posada-Bedoya[1], Andrés Gómez-Giraldo[2], Ricardo Román-Botero[3]

DRAFT

February 2024

Running head: Vertically propagating seiches

[1,2,3]Department of Geosciences and Environment, Universidad Nacional de Colombia, Calle 59A No 63-20, Medellín, Colombia.

[1]Now at Department of Civil Engineering, Queen's University, Kingston, Ontario, ON K7L 3N6, Canada

[1]Corresponding author. Email: 21afpb@queensu.ca

[2]Email: eagomezgi@unal.edu.co

[3]Email: rroman@unal.edu.co

Keywords: vertical propagation, standing waves, supercritical reflection, steep lake

Abstract

This work investigates observations of gradual upward phase shifting of temperature oscillations in a steep tropical reservoir, which differ from the π radians sharp shifts that are usually accepted for the description of baroclinic motions in terms of normal modes. Supported on numerical modeling and theoretical inviscid wave ray tracing, we show that the gradual upward phase shifting is the signature of vertically propagating seiches, which refer to basin-scale oscillations that are stationary in the horizontal but propagate downwards in the vertical. We show that the vertically propagating seiche occurs due to the predominant supercritical reflection of the internal wave rays at the lake boundaries, which focuses the internal wave energy downwards with a minor fraction of the energy reflected upwards, resulting in a net downward energy propagation. The net downward energy flux precludes the formation of standing waves, with potential implications for the common framework of the energy flux path at the interior of stratified lakes. The analysis supports that vertically propagating seiches and standing mode preclusion are expected to occur in any given lake, but their signatures are more evident in steep sided lakes, with a wide metalimnion and/or for lower forcing frequencies, characteristic of higher order vertical modes.

Plain Language Summary

In stratified lakes, large scale perturbations like those generated by the wind propagate as internal waves, with oscillatory motions of the particles that propagate in trajectories forming an angle with the horizontal. When they bounce at the lake contour, change direction but keep the angle of propagation respect to the horizontal plane. Incident and reflected waves

superpose and, under the ideal condition of no energy losses, form stationary basin scale internal waves, with points where there are no oscillations of the particles, which are called nodes. Although there is some energy loss along the propagation of the waves, in several cases they are small and natural mode theory describes the reality closely, so it is common to describe basin-scale periodic motions in terms of standing waves. We investigated observations of oscillatory basin-scale motions in a steep-sided tropical reservoir that are not stationary but have nodes that propagate upwards, which is a signature of wave energy propagating downwards. We show that this is the result of the reservoir sides being steeper than the trajectories of propagation of the waves, leading to accumulation of energy in the lake bottom instead of a reflection that allows for stationary waves to form.

Key points

- Net downward internal wave energy flux can occur in stratified lakes due to the imperfect reflection of internal wave rays.
- Predominant supercritical reflection of the internal wave rays at the lake boundaries results in a net downward energy propagation.
- Net downward energy propagation is more evident in steep lakes, lakes with a wide metalimnion and/or at lower forcing frequencies.

1. Introduction

The classical interpretation of coherent basin-scale internal motions in stratified lakes and reservoirs has been based on the decomposition onto its natural non-dissipative oscillation modes. This approach has been useful to understand the complex field of baroclinic motions at the basin scale and their energy flux path through the interactions of modes with the topography (Kocsis et al. 1998; Vidal et al. 2013), between modes (de la Fuente et al. 2008, 2010), with the bottom boundary layer (Lemckert et al. 2004; Simpson et al. 2011) and with the turbulent field (Boegman et al. 2003; Gómez-Giraldo et al. 2008; Ulloa et al. 2015), which finally impact water quality through mixing and transport (Evans et al. 2008; Pernica et al. 2013).

Strictly speaking, pure non-dissipative modes do not exist in real sloping bottom lakes (Shimizu and Imberger 2008) because the irregular bathymetry creates some residual unbalance between focusing and defocusing of some wave rays so they do not close upon themselves (Maas and Lam 1995; Thorpe 1998). Focusing of wave rays also concentrates energy and enhances viscous dissipation so the reflected rays have less energy than the incident rays, resulting in some degree of energy net downward propagation as upward and downward propagating rays do not have the same energy. In some cases, the energy net vertical flux is negligible, and the internal mode approach leads to good agreement with observations (Shimizu and Imberger 2008; Imam et al. 2013), while in other cases such approach is unable to approximate some characteristics of the oscillatory internal motions (Henderson and Deemer 2012). For instance, the internal mode approach predicts sharp changes of phase through the water column, while gradual changes of phase have been observed in several reservoirs (Lazerte 1980; Vidal and Casamitjana 2008; Henderson 2016).

Therefore, it is very pertinent to understand when the classical description of the oscillatory motions in terms of modes is inappropriate and should be precluded, and what else is necessary to better understand and describe the energy flux path at the interior of lakes (Imberger 1998; Wüest and Lorke 2003).

The bulk of research on baroclinic oscillations has focused on natural mild slope lakes, with predominant subcritical slopes, where most of the downward propagating energy introduced by the wind is reflected upwards at the bottom, allowing for standing waves formation. In those cases, the internal wave field can be well described in terms of the non-dissipative modes and perfect reflections can be considered. Conversely, in steep bottoms systems, slopes may be mostly supercritical and focus wave energy downwards upon reflection, reducing the upward wave energy available for the interference necessary to produce standing modes, so the resulting basin-scale oscillations after superposition are stationary in the horizontal but propagate downwards in the vertical, and standing waves do not develop, as first hypothesized by Thorpe (1998) and evidenced by Henderson and Deemer (2012). Following Henderson and Deemer (2012) and Henderson (2016), we call them vertically propagating seiches. In such a case, an upward phase shifting with depth of the temperature and velocity fluctuations is a clear signature of downward energy flux (Henderson and Deemer 2012). As steep lakes have been far less studied, the robustness of the non-dissipative mode model has not been thoroughly explored, so it is important to investigate conditions for its preclusion and identify the characteristics of the vertically propagating seiches when the mode is not formed.

This work is motivated by observations and numerical modeling in a steep reservoir that showed a coherent gradual vertical shifting in the phase of horizontal mode one basin-scale

oscillations with depth, very different from the π radians sharp shifts that are usually accepted for the description of baroclinic motions in terms of normal modes. Supported on numerical modeling and theoretical tracing of wave rays, we identify these motions as vertically propagating net oscillations, produced by the superposition of downward propagating waves and upward propagating reflected waves which are less energetic due to the dominant supercritical reflection of internal waves at the lake sloping bottom. We discuss the role of the sloping bottom on the standing mode preclusion and provide some context of our results respect to other lakes, supported on previously proposed parameterizations.

2. Theoretical background

Inviscid internal waves in a stratified fluid can be seen as a set of rays, whose energy propagates at an angle θ respect to the horizontal, depending on the background stratification, characterized by the buoyancy frequency N, and wave frequency , ω:

$$\sin\theta = \frac{\omega}{N} \tag{1}$$

The fluid particle velocity $\vec{u}$ is orthogonal to the phase velocity $\vec{c}_p = \omega/\vec{k}$, where $\vec{k}$ is the wavenumber vector. The direction of energy propagation coincides with the direction of the particle motions, so the group velocity $\vec{c}_g$ and $\vec{c}_p$ are orthogonal with opposite vertical components (Turner 1973), such that downward (upward) wave energy flux is accompanied by upward (downward) phase propagation (Figure 1).

Internal wave rays maintain their propagating angle with the horizontal plane (θ) upon reflection at a solid boundary (Maas and Lam 1995), so incident and reflected rays make different angles to the sloping bottom, leading to wavelength change upon reflection (Fig. 1).

A decrease in wavelength after reflection is known as focusing (Fig. 1a, c) and a increase as defocusing (Fig. 1b, d). When the bottom slope α is milder than that of the ray ($\alpha < \theta$), the reflection is subcritical and the ray shifts its vertical direction of propagation upon reflection, so downward propagating waves are reflected upwards (Fig. 1a, b). If the boundary slope is steeper than the ray ($\alpha > \theta$), downward propagating rays continue traveling downwards upon reflection (Fig. 1c, d). When wave energy propagation and bottom slopes are similar, i.e. close to the critical condition, large wave energy concentration (focusing) leads to a large amplitude reflected wave which turns into turbulence by overturning instability (Dauxois et al. 2004), with large wave energy loss, so the reflected wave is far less energetic than the incident one.

Standing waves occur when opposite identical progressive waves interfere. Because of the inclined paths of individual wave rays in stratified flows (eq. 1), the condition for standing modes to form is that every wave ray closes upon itself after bouncing from the boundaries (Fig. 1e) (Cushman-Roisin et al. 1989; Maas and Lam 1995). Moreover, because of the irregular bottom in natural basins, for a given forcing frequency there are always some rays that do not close upon themselves, so standing wave excitation is not perfect, and some degree of energy downward propagation always remains. Also, viscous dissipation and transference to turbulence reduces energy in the waves as they travel through the basin and bounce at the boundaries, so the upward reflected waves are less energetic, and upon interference with the downward waves, a residual downward propagation remains. These energy losses are small in mild slope natural lakes with significant subcritical reflection (Wiegand and Chamberlain 1987; Münnich et al. 1992; Imam et al. 2013). In some cases, most of the wave rays can be trapped by successive reflections at the boundaries towards

particular regions of the basin, like the shore or the bottom, and no longer close upon themselves, precluding standing waves (Thorpe 1998). In particular, when supercritical reflection is dominant, wave rays are focused towards the bottom and a minor fraction of energy is reflected upwards to conform the standing wave such that downward propagating waves dominate because of the difference in downward and upward energy fluxes (Fig. 1f) (Henderson and Deemer 2012).

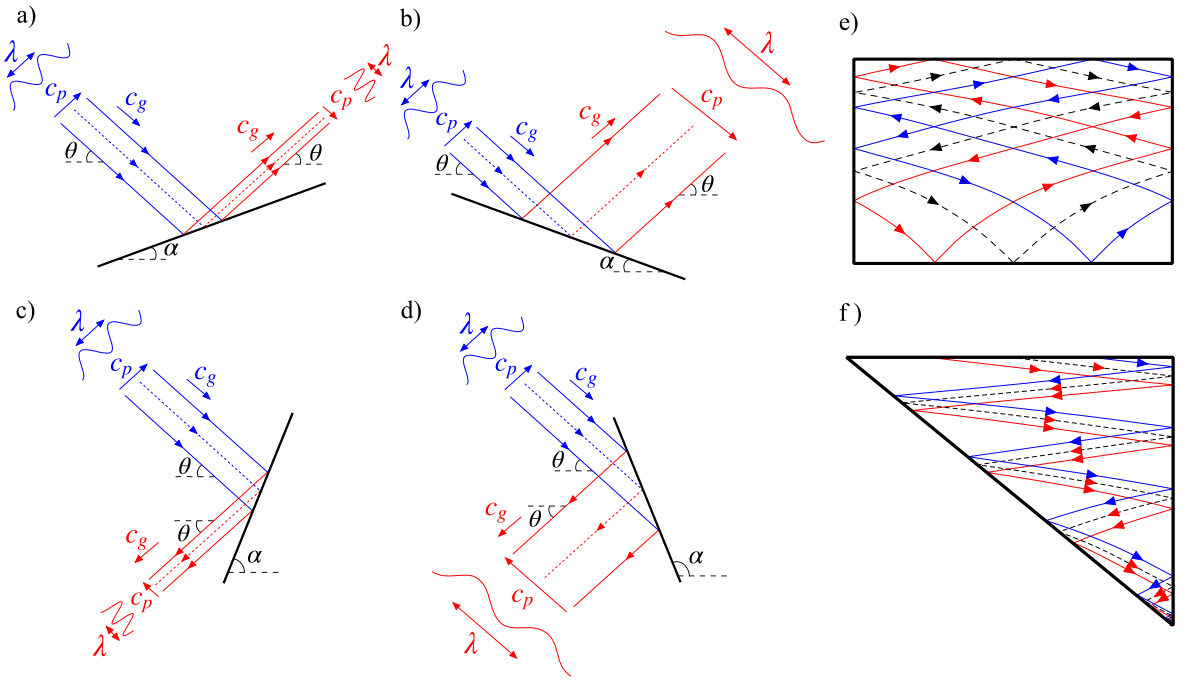

Figure 1. Schematic of wave rays reflecting at a (a, b) subcritical and (c, d) supercritical solid boundary (a, c) focusing and (b, d) defocusing. Blue and red lines denote the lines of constant phase of incident and reflected waves respectively and arrows indicate the direction of energy propagation. Dashed and continuous lines indicate trough and peaks of the wave respectively. Schematic of wave ray paths for (e) a standing mode (every wave ray closes upon itself) and (f) vertically propagating seiche in a supercritical basin (wave rays are trapped at the bottom).

3. Materials and methods

3.1. Study site and field measurements

La Fe is a tropical reservoir located in the Northwest of Colombia (06◦06’40”N, 75◦30’00”W) at 2150 m.a.s.l. on the Andean Mountain range (Fig. 2). This tropical Andean reservoir remains thermally stratified through the year, with seasonal changes ruled by the inflow discharge (Román-Botero et al. 2013; Posada-Bedoya et al. 2021; Posada-Bedoya et al. 2022). The reservoir is composed of two basins (North and South) separated by a shallow and narrow neck formed by the old-submerged dam Los Salados.

After Posada-Bedoya et al. (2022) showed that internal oscillations in each basin are decoupled, we will focus here on the South basin, where a LakeESP platform equipped with a thermistor chain and a meteorological station was installed close to the dam site (Fig. 2) to collect data every 5 min from 6 to 22 September 2012. Thirteen temperature loggers were hanging from the float at depths of 0.7, 1.5, 2.3, 3.0, 3.8, 4.5, 5.3, 6.1, 7.3, 9.1, 11.2, 13.2, 15.2 m, and one additional thermistor was moored 1 m above the lake bottom. Temperature loggers had a resolution of 0.0001°C and an accuracy of 0.01°C. The meteorological station measured air temperature, atmospheric pressure, relative humidity, net shortwave and longwave radiation, rainfall, and wind speed and direction.

The periodic wind excites 24, 12 and 6-h basin-scale horizontal mode 1 oscillations in the South basin that are decoupled and have different vertical structure in both basins of the reservoir (Posada-Bedoya et al. 2022). The more energetic mode shows a vertical structure that resembles that of a stationary vertical mode 4, so it could be classified as a V4H1 mode. However, sharp phase changes between layers, as are predicted by normal modes, were not observed and a coherent gradual shift with depth in the phase was observed instead.

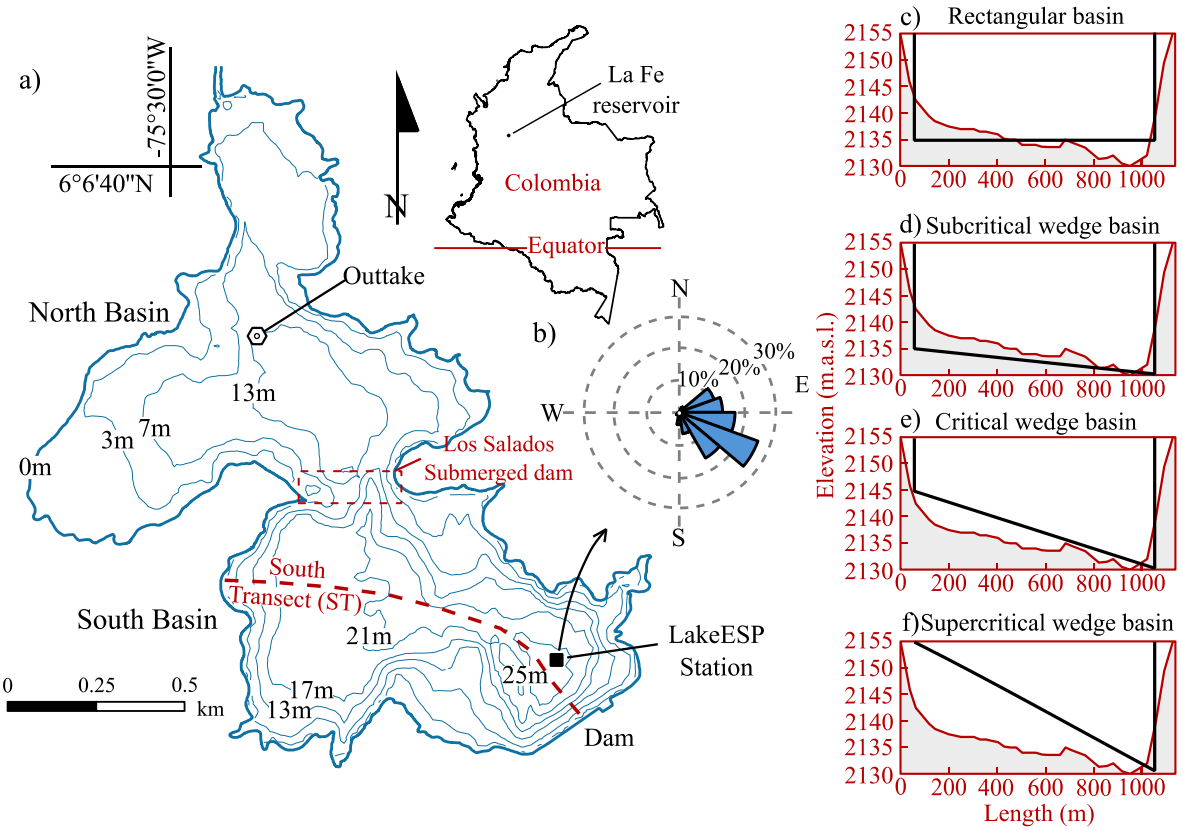

187

188 **Figure 2.** (a) Location and bathymetry of La Fe reservoir and LakeESP station location. (b)
189 Wind rose for wind speeds faster than 2.5 m s^{-1}. (c-f) Bottom elevation along the South
190 transect shown in (a) (red line) and wedge basins for numerical experiments (black line).

191

192 3.2. Hydrodynamic modeling

193 Numerical experiments with the 3D hydrodynamic model AEM3D were conducted to
194 understand the nature of the diurnal oscillations in La Fe South basin, and to explore the
195 effect of the sloping bottom.

196

3.2.1. AEM3D model

The Aquatic Ecosystem Model (AEM3D) (Hodges and Dallimore 2016) solves the three-dimensional (3D), hydrostatic, Boussinesq, Reynolds-averaged Navier-Stokes equations, and scalar transport equations in a z-coordinate system, using a finite-difference discretization of momentum and a finite-volume discretization of conservation of mass (Hodges 2000; Hodges and Dallimore 2016). The free surface evolution is modeled implicitly, while advection of momentum and scalars are solved explicitly with an Euler-Lagrangian scheme and an ULTIMATE-QUICKEST scheme, respectively (Hodges 2000; Hodges and Dallimore 2016). The model uses UNESCO (1981) equation of state to relate temperature and density. The mixed-layer algorithm computes vertical mixing throughout the water column based on an integral model of the turbulent kinetic energy equation (Hodges 2000). Horizontal mixing is solved through an eddy viscosity model. No-slip and zero normal flow boundary conditions are imposed at bottom and lateral boundary cells. Because of the staircase representation of the bottom, the model slightly overestimates numerical diffusion and internal wave damping (Gómez-Giraldo et al. 2006; Vidal et al. 2013), despite which it has been demonstrated to accurately predict basin-scale internal waves in a wide variety of lakes and reservoirs worldwide (Vidal et al. 2013; Woodward et al. 2017; Dissanayake et al. 2019).

3.2.2. Numerical experiments

After calibration of the AEM3D model with temperature records from a thermistor chain (Posada-Bedoya et al. 2021), we conducted five two-dimensional numerical experiments: one for a basin with the bottom profile of the decoupled South basin (South Transect in Fig. 1) and the other four for idealized vertical walls wedge-shaped basins with different bottom

slopes (Fig. 2c-f). To simulate 2D basin geometries with the 3D model, we setup the bathymetry of each scenario in the x-z plane (Fig. 2c-f), with an individual cell in the spanwise direction and a free-slip boundary condition on the sidewalls. Results were insensitive to the spanwise cell size.

For each scenario, the domain was discretized using a uniform horizontal grid of 25 m and 0.4 m uniform thick layers (Table 1). We verified grid independency of the results at this spatial resolution. The time step was 10 s to meet the numerical stability condition for the internal motions. We simulated the response in each case to the forcing of an idealized wind with a speed $v = v_0 cos(\omega t)$, with $v_0 = 3$ m s^{-1} and a frequency $\omega = 7.27\times10\text{-}5$ s^{-1} (24 h period) in the case with the shape of the South basin, as it was the period of the dominant oscillations observed in the field (Posada-Bedoya et al. 2022). For the idealized wedge basins, the forcing period was 20 h, which is the period of the theoretical V4H1 mode of the rectangular basin, according to Gill (1982) eigenmodel for the average stratification of the survey (Fig. 3b). We ran the model without other external forcing, i.e. with no other meteorological inputs than the wind, inflows, or outflows. By simulating the basins with a perfectly periodic wind forcing, we are considering the most favorable condition for the standing mode excitation in each case. The model ran for 9 days, enough time for the excitation of a standing wave, before mixing modifies the background stratification and the natural modes characteristics. The model was initialized with the average stratification of the survey (Fig. 3b), with horizontally homogeneous layers and zero velocity everywhere. The simulations were carried out using default model parameters, which were based on non-site-specific literature values (Hodges and Dallimore 2013), as in other modelling studies (Woodward et al. 2017).

Based on the forcing period of the idealized wedge scenarios and the minimum value of the buoyancy frequency (N_{min} =0.0057 Hz) (Fig. 3b), the critical slope ($\theta_c = 2\pi\omega/N_{min}$) was 0.0153 rad, on which we relied to define the bottom slope of the wedges (α) as subcritical ($\alpha < 0.7\theta_c$), critical ($0.7\theta_c < \alpha < 1.5\theta_c$) and supercritical ($\alpha > 1.5\theta_c$), similar to what was used in previous studies (Gómez-Giraldo et al. 2006; Henderson and Deemer 2012) (Table 1).

Table 1. Parameters for the setup of numerical experiments.

Scenario	α (rad)	α/θ_c	Maximum depth H (m)	Length L at H/2 depth (m)
Rectangular	0.000	0.00	20	1000
Subcritical	0.005	0.33	25	1000
Critical	0.015	0.98	25	850
Supercritical	0.025	1.63	25	500
South basin	----	----	27	1100

3.2.3. Analysis of model results

The vertical structure of the oscillations was identified from calculations of wavelet coherence and phase (Grinsted et al. 2004) for series of temperature profiles close to the deepest edge of the basin, and by band-pass filtering the time series of horizontal velocity profiles predicted by the 3-D model using a fourth-order Butterworth filter.

3.3. Wave ray tracing

For each scenario, we traced the path in the time-depth (t-z) space of constant phase lines of linear shallow water progressive WKB waves (Phillips 1977). At a fixed horizontal position, wave crests move vertically at speed $c_z = \omega/k_z$ (Sutherland 2010), so constant phase lines paths are given by

$$\frac{dz}{dt} = c_z = \frac{2\pi\omega^2\lambda_x}{N(z)} \quad (5)$$

where λ_x is the horizontal wavelength and k_z is the vertical component of the wavenumber vector. We traced constant phase lines every $T/2$ by solving eq. 5 at discrete time steps, starting at the bottom in the center of the basin. We compared the path of constant phase lines to the time-depth structure of the band-passed simulated horizontal velocity, accepting that a close agreement indicates vertical propagation Henderson and Deemer (2012). In all the wedge cases, the stratification and forcing frequency were the same, thus the differences in the paths were only due to the selected wavelength λ_x, in this case $2L$, as the basin-scale waves observed in the lake are horizontal-one (Posada-Bedoya et al. 2022), and L being the length of the basin at the middle depth (Table 1). The path of wave ray energy in the length-depth (x-z) space of each basin for the given forcing frequency was calculated from:

$$\frac{dz}{dx} = \tan\theta \quad (6)$$

Differences in wave energy paths in the wedge basins were only due to the basin geometry, which determines the distance traveled by wave rays at different depths as they repeatedly cross the lake and reflect from end walls while propagating from surface to bed (or from bed to surface). Energy wave packet was not traced in the south basin because the wave ray propagation occurs in a three-dimensional space.

3.4. Reflection coefficient

The reflection coefficient is the fraction of incident wave energy that is reflected at the lake bottom (Henderson and Deemer 2012; Henderson 2016). The closer it is to one, the closer

281 the superposition of down and upward propagating waves is to a standing wave or natural
282 mode. In this work, it was calculated for each numerical experiment by adjusting the
283 theoretical interference pattern between downward (incident) and upward (reflected)
284 progressive waves to that of the modeling results. We estimated vertical profiles of power
285 and phase $\hat{\psi}_M(z,\omega_0)$ of the internal wave forced at frequency ω_0 in AEM3D by computing
286 the Fourier transform $\hat{\psi}_M(z,\omega)$ of the horizontal velocity signal $u_M(z,t)$, simulated at
287 several heights (z) in the center of the basin:

$$u_M(z,t) = \sum_{\omega} \hat{\psi}_M(z,\omega) e^{i2\pi\omega t} \tag{2}$$

288 The theoretical profile of power and phase $\hat{\psi}_T(z,\omega_0)$ for the wave forced at the frequency
289 ω_0 was estimated as in Henderson (2016):

$$\hat{\psi}_T(z,\omega_0) = \left(\frac{N(z)}{N_0}\right)^{1/2} \hat{\psi}_{z_0}\left[e^{-i\phi_T(z,\omega_0)} + Re^{i\phi_T(z,\omega_0)}\right] \tag{3}$$

290 where R is the reflection coefficient, $\hat{\psi}_{z_0}$ is the complex amplitude of downward-propagating
291 waves at the height of reference z_0, $N_0 = N(z_0)$, and the theoretical phase between $\hat{\psi}_{z_0}$ (at
292 z_0) and $\hat{\psi}_T(z,\omega_0)$ at elevation z is:

$$\phi_T(z,\omega_0) = \int_{z'=z_0}^{z} \frac{2\pi}{\lambda_z} dz' = \int_{z'=z_0}^{z} \frac{N(z')}{\omega_0 \lambda_x} dz' \tag{4}$$

293 where λ_x and λ_z are the horizontal and vertical projections of the wavelength respectively.
294 We adjusted simultaneously R, λ_x and $\hat{\psi}_{z_0}$ by minimizing the squared error between
295 $\hat{\psi}_T(z,\omega_0)$ and $\hat{\psi}_M(z,\omega_0)$ profiles, for ω_0 associated to the forcing period in each case. We
296 used AEM3D results above 15 m deep in the center of the basin, as below that depth the wave
297 rays are nearly vertical because of the reduced stratification (Fig. 3b), so the vertical

298 wavelength grows exponentially (eq. 4) and the energy profile is roughly uniform, similarly
299 to Henderson (2016).

300

301 **4. Results**

302 4.1. Overview of field and model results

303 The background temperature vertical structure did not change significantly throughout the
304 survey (Fig. 3a) and had a relevant gradient from the near surface down to ~14 m deep, and
305 was nearly uniform below that depth (Fig. 3b). The wind speed exhibited a strong diel
306 variability with the strongest winds coming from the East-Southeast (Fig. 1b) early in every
307 afternoon and forcing internal waves with dominant periods of 24, 12 and 6 h in the South
308 basin (Fig. 3c) oscillating along the east-west transect and being decoupled from those in the
309 North basin (Posada-Bedoya et al. 2022). The 24-h oscillations exhibited a continuous phase
310 shifting with depth in the top 15 m, gradually reversing direction (changing phase by $\pi/2$
311 radians) three times in both field and model results (Fig. 3d, g), which is indicative of vertical
312 propagation of wave energy. The internal waves of 12-h and 6-h period exhibited structures
313 resembling V2 (Fig. 3e, h) and V1 (Fig. 3f, i) oscillations.

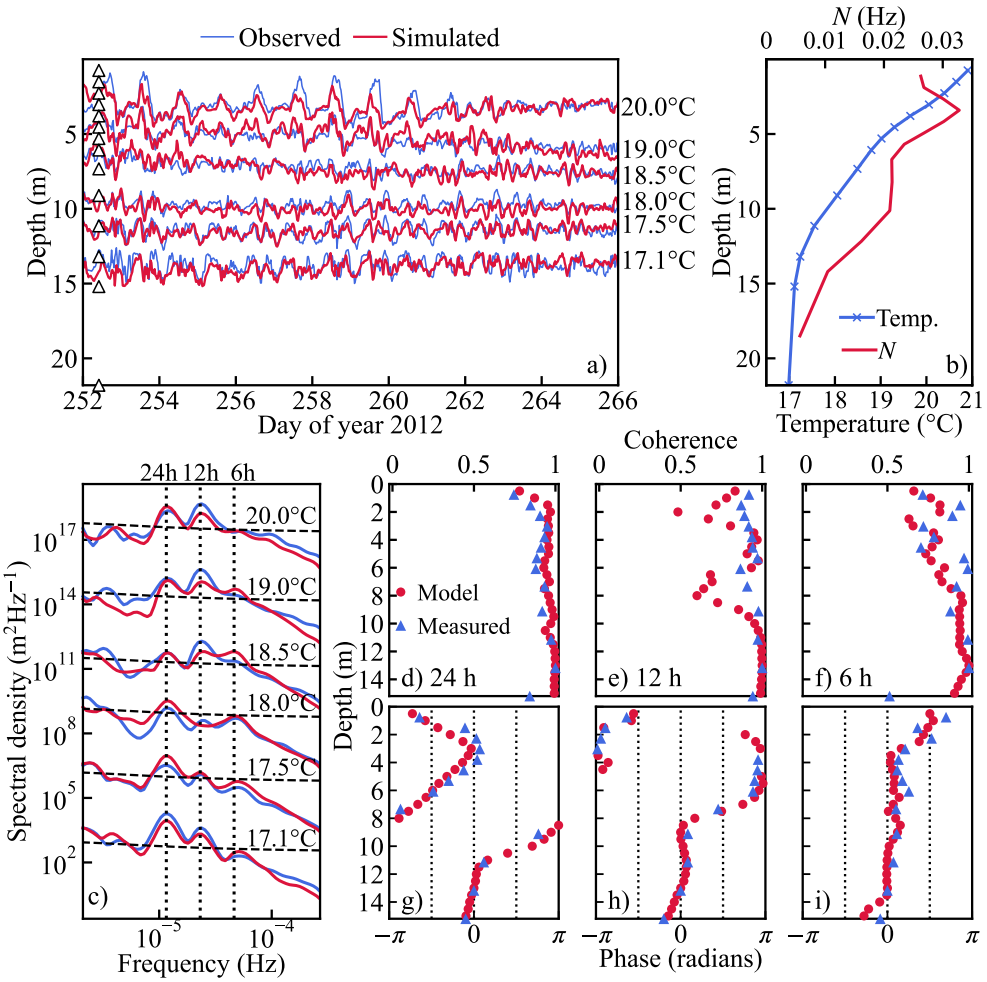

314

315 **Figure 3.** (a) Isotherm depths estimated from measurements and model results. The triangles
316 indicate the depth of the thermistors. (b) Average temperature and buoyancy frequency
317 profiles. (c) Global wavelet spectra of the observed (blue lines) and modeled (red lines)
318 isotherm displacements. Dashed line indicates the threshold for significant energy with a
319 95% confidence. Offset between spectra is three logarithmic cycles. Profiles of wavelet (d,
320 e, f) coherence and (g, h, i) phase of the temperature fluctuations of (d, g) 24 h, (e, h) 12 h
321 and (f, i) 6 h period oscillations. Coherence and phase are relative to the 13 m deep
322 temperature signal.

323

4.2. Periodically wind-forced basins

We define $2t_{ray}$ as the time required for wave energy to travel downwards from the surface, bounce at the bottom and return to the surface. In all the scenarios, before a time $\sim 2t_{ray}$, the phase profile of temperature oscillations exhibited a continuous upward shifting (Fig. 4d), indicating that before a time $\sim 2t_{ray}$ the wave energy fluxed downwards as in a progressive wave, excited by the first cycle of wind forcing. Unlike vertically standing modes, the band-passed horizontal velocity in the time-depth space showed upward phase propagation matching the theoretical upward propagation of constant phase lines (Fig. 4b).

In the rectangular and subcritical basins, from a time $\sim 2t_{ray}$ onwards the horizontal velocity in the time-depth space exhibited the arrangement of oscillating cells, characteristic of a standing mode (Fig. 4b1, b2 and Supplementary Videos 1 and 2). The coherence of temperature oscillations decreased at depths where phase shifts close to π radians occurred, suggesting the presence of nodes of vertical displacements in a standing wave (Fig. 4 c1, c2, d1, d2). The ray tracing predicted wave rays closing upon themselves for wave periods of 19.4 and 18.9 h for rectangular and subcritical cases respectively (Fig. 4a1, a2), after bouncing four times at each lateral wall, in agreement with the estimated V4H1 mode of 20-h period of the rectangular basin.

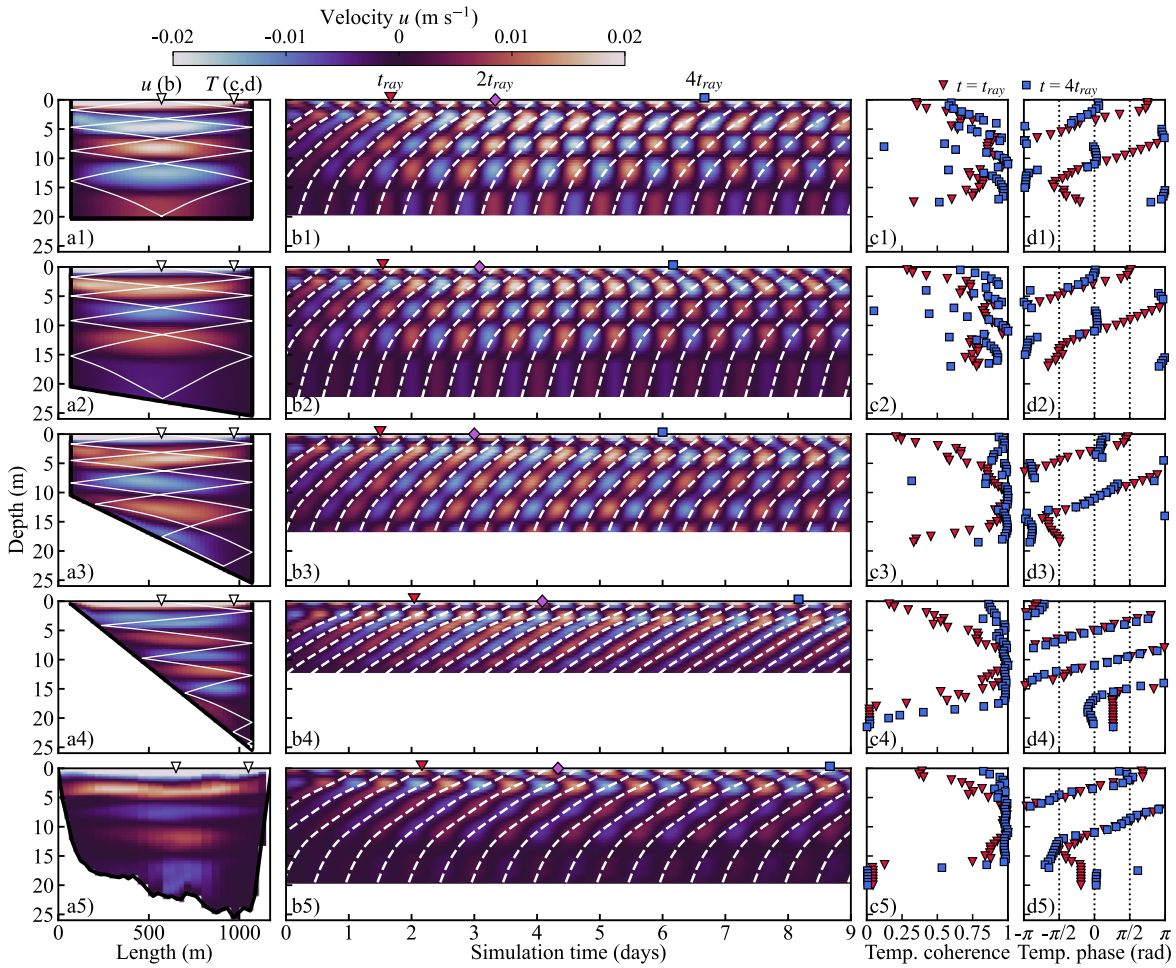

341

342 **Figure 4.** (a) Depth-length curtain of band-passed horizontal velocity at a time of maximum
343 kinetic energy. Panels 1-5 are respectively for rectangular, subcritical, critical, supercritical
344 and South basins. The white line in panels a1-a4 is the path of an energy wavepacket excited
345 at the center of the lake surface. (b) Time-depth contours of the band-passed horizontal
346 velocity in the center of the basin. White dashed lines show the path of theoretical constant
347 phase lines. Profiles of (c) coherence and (d) phase of temperature oscillations at the deepest
348 part of the basins (location indicated in panels a), at the times indicated by markers in panels
349 (b). Coherence and phase are relative to the 10 m deep temperature signal.

350

In the supercritical case the horizontal velocity structure in the time-depth space showed upward phase propagation consistent with the theoretical constant phase lines of progressive waves for the entire simulation (Fig. 4b4 and Supplementary Video 4). The coherence of temperature oscillations was high throughout the water column (Fig. 4c4), so nodes and antinodes characteristic of a standing wave did not occur, contrasting with the nodes and antinodes observed in the rectangular and subcritical cases. The continuous upward phase shifting remained throughout the simulation very similar to that before $2t_{ray}$ (Fig. 4d4), suggesting a permanent downward propagation of energy and that standing modes of 20-h period were not formed, despite the ideal periodic forcing conditions for their excitation. The ray tracing in the x-z space showed the continuous downward reflection at the boundaries and the consequent trapping of the wave energy at the bottom of the basin for waves of 20 h period (Fig. 4a4). The oscillations had a vertical structure higher than V4, due to the increase in the number of times the ray crosses the lake from side to side (Fig. 4a4), as the vertical wavelength ($\lambda_z = 4\pi\omega L/N$) is shorter because of the smaller L.

The nearly critical case was a transitional condition between subcritical and supercritical cases. The phase showed a hybrid structure with $\sim \pi$ radians shifts at some depths and upward shifting between 7 and 14 m (Fig. 4d3 and Supplementary Video 3). The coherence reductions were less marked than in the rectangular and subcritical cases (Fig. 4c3), even after several cycles of wind forcing, so nodes were not clearly developed. The wave ray closed upon itself for a period of 20.2 h, but propagated nearly parallel to the sloping bottom after reflection (Fig. 4a3), so the inviscid ray tracing is expected to be invalid because of the large dissipation associated to the instabilities associated to the nearly critical reflection expected in this region (Dauxois et al. 2004).

In the south basin experiment, as in the supercritical case, the horizontal velocity structure in the time-depth space did not develop the cell structure associated to standing modes, and instead, it kept the progressive wave signature, fitting the theoretical phase of progressive waves throughout the simulation (Fig. 4b5 and Supplementary Video 5). The phase structure of temperature oscillations maintained a gradual upward shifting (Fig. 4d5) like the one obtained from field measurements and the 3D simulation (Fig. 3g). Coherence was high throughout the water column, indicating nodes and antinodes did not occur (Fig. 4c5). According to this, despite the ideal periodic wind forcing, the standing mode of 24 h period was not formed and instead a vertically propagating internal seiche was excited. A very similar result was obtained when the system was forced with a 20-h period wind (not shown). As in the field and model validation, the phase profile reverses its slope around the depth of maximum N ($\sim$3 m), in agreement with the relation between phase and buoyancy frequency in eq. 4.

4.3. Reflection coefficient

The theoretical pattern of interfering progressive waves fits very well to the power and phase profiles estimated from AEM3D results (Fig. 5), so the adjusted R and λ_x (Table 2) are reliable. The reflection coefficient is higher for the rectangular and subcritical cases and reduces dramatically for the supercritical scenario, while the nearly critical case poses a transition between both conditions. In the real bathymetry of the south basin, the reflection coefficient was between those for the critical and supercritical cases, in accordance with the signatures of vertical propagation shown above. The adjusted λ_x was always very close to $2L$ (cf. L at $H/2$ depth in Table 1 to λ_x in Table 2), consistent with the horizontal-one

oscillations. Nodes and antinodes of a standing wave can be identified in the rectangular and subcritical cases but are less evident as the bottom slope increases and in the south basin.

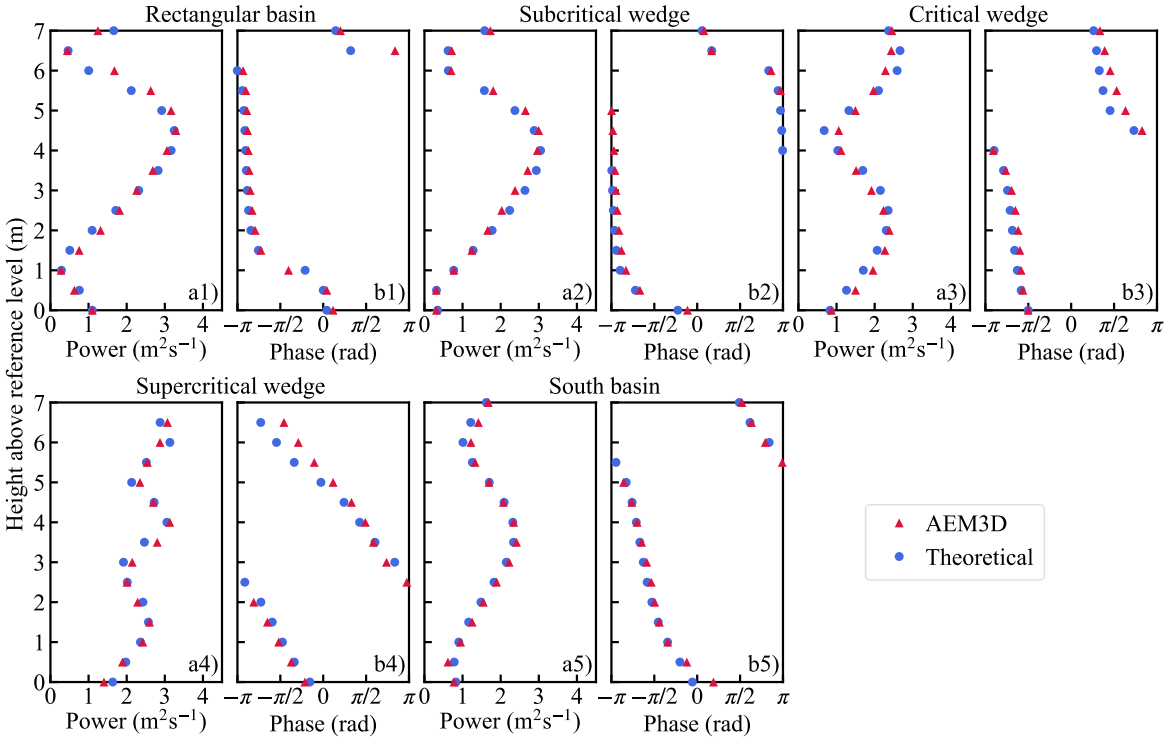

Figure 5. Power and phase profiles estimated from AEM3D results and from theoretical interference between opposite progressive waves.

Table 2. Fitted reflection coefficient $\boldsymbol{R}$ and horizontal wavelength $\boldsymbol{\lambda_x}$ for each scenario.

Scenario	α/θ_c	R	λ_x (m)
Rectangular	0.00	0.89	2000
Subcritical	0.33	0.85	2187
Critical	0.98	0.62	1711
Supercritical	1.60	0.14	1037
South basin	----	0.42	2378

5. Discussion

5.1. Role of the sloping bottom on the vertical propagation

Numerical experiments indicate that diurnal standing waves were precluded in La Fe South basin and, instead, a 24-h period vertically propagating horizontal mode one seiche was observed. Comparing the slopes of the wave ray path (calculated with eq. 1 for the measured average buoyancy frequency at the bottom) and the bottom, we classified the reflection as subcritical ($\alpha < 0.7\theta_c$), critical ($0.7\theta_c < \alpha < 1.5\theta_c$) or supercritical ($\alpha > 1.5\theta_c$) (Fig. 6a), and found that most of the reflections of 24-h period waves in the south basin are supercritical, explaining why a downward vertically propagating seiche is observed instead of a standing vertical mode. Because of the predominant supercritical reflection, internal wave energy is focused and trapped at the bottom, where it is expected to be the main source of energy for the bottom boundary layer, as in Henderson (2016), differing from the common framework of the energy flux path at the interior of stratified lakes (Imberger 1998; Wüest and Lorke 2003), with potential implications for mixing and transport processes that impact water quality.

As the forcing frequency increases, the area where reflection is subcritical grows (Fig. 6) and more energy can be reflected upwards at the sloping bottom and standing waves can be observed. This is illustrated by forcing the south basin with 6-h period winds, which excite a coherent V1H1 response (Fig. 7) (Supplementary Video 6). Increasing supercritical reflection for lower forcing frequencies implies that higher order vertical motions are more likely to occur as vertically propagating seiches and are less suitable to be described as standing modes. This is consistent with the gradual phase shifting in the temperature and

velocity profiles, observed more often in lakes with dominant oscillations of high vertical order (Lazerte 1980; Serra et al. 2007; Henderson and Deemer 2012).

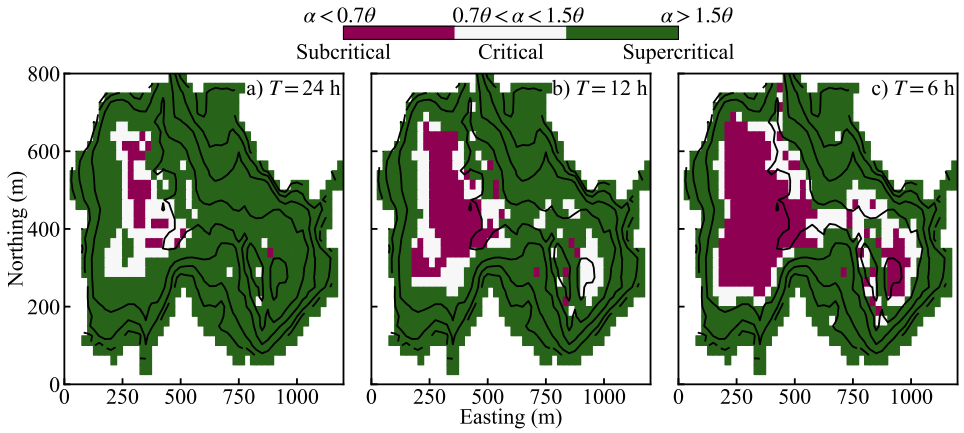

Figure 6. Spatial classification of the sloping bottom of the South basin for wave periods of (a) 24, (b) 12 and (c) 6 h.

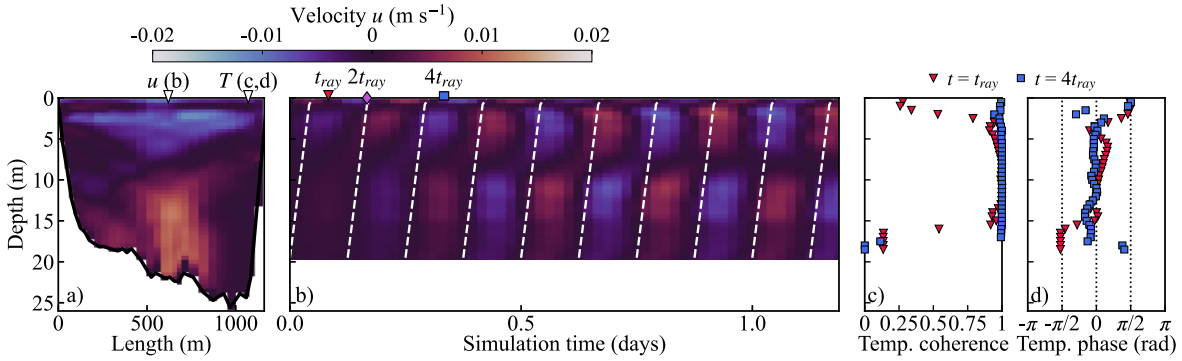

Figure 7. Response of the South basin to a 6-h period forcing: (a) Curtain along the south transect (ST) of band-passed horizontal velocity after one day of simulation, (b) Time-depth contours of the band-passed horizontal velocity in the middle of the basin, with white dashed lines showing the path of theoretical constant phase lines. (c) Coherence and (d) phase of temperature profiles at the deepest edge of the basin (panels a) at the times indicated by markers in panels (b).

5.2. Ubiquity of vertically propagating seiches

The reflection coefficient for the rectangular and subcritical cases was slightly lower than 1, indicating that the reflected energy was lower than the incident and a net residual downward energy propagation occurred, despite clear signatures of standing waves being identified in those cases. This shows that some degree of vertical propagation of basin-scale internal waves should always be expected, even in the simplest rectangular basin. Still, a large bulk of research has been conducted using the inviscid natural mode concept to describe basin-scale internal waves in lakes (Wiegand and Chamberlain 1987; Münnich et al. 1992; Imam et al. 2013).

We conjecture that vertically propagating seiches have not been widely explored because systems with adequate conditions for them to be clearly evident, like steep walls and wide metalimnion, have been far less studied. Most descriptions of basin-scale internal waves have been conducted in natural mild slope lakes, where a significant subcritical reflection occurs such that appreciable standing waves develop even if some small degree of vertical propagation remains, and in temperate systems with a thin metalimnion. In the latter case, the stratification is weak above (in the surface layer) and below (the hypolimnion) of the thin metalimnion, so wave ray paths are nearly vertical in those regions of the water column, and the phase shifting is mainly confined to within the thin metalimnion, making it difficult to distinguish the gradual phase shifting when occurring. Instead, in systems with a wide metalimnion, the signature of the gradual phase shifting with depth extents through a larger depth range, so it is more evident when occurring, as in some shallow summer temperate lakes (Lazerte 1980), temperate reservoirs with selective withdrawal at intermediate depths

(Serra et al. 2007), or tropical Andean reservoirs during moderate dry conditions (Posada-Bedoya et al. 2019).

To provide a global context of the degree of vertical propagation in La Fe, in comparison with other lakes, we estimated the parameters $D = NH/(\pi\omega L)$ (Henderson and Deemer 2012) and reflection coefficient $\mathcal{R}$ (Henderson 2016), defined in terms of readily available variables measured in the field, for several systems where high order vertical modes were dominant (Table 3). The parameter D is the ratio of mean lake ($2H/L$) to wave ray ($2\pi\omega/N$) slopes. High values of D are typical of steep and/or strongly stratified lakes, with dominant supercritical reflection and vertical propagation, and low values are typical of mild slope and/or weakly stratified lakes, with a dominant subcritical reflection that favors standing waves excitation. The parameter $\mathcal{R}$ is a parameterization of the reflection coefficient R in terms of readily available variables measured in the field. It was estimated as (Henderson 2016):

$$\mathcal{R} = \frac{1-\beta}{1+\beta} \tag{8}$$

$$\beta = 2\left(\frac{8}{\pi}\right)^{1/2} C_D \frac{v_{RMS}}{c_{gz}} \tag{9}$$

where C_D is the bottom drag coefficient, v_{RMS} is the root-mean-square of the velocity of the internal waves induced currents, and $c_{g,z}$ is the vertical component of the group velocity, with the same magnitude of the vertical phase velocity in eq. (5). A value of $\mathcal{R}$ =1 indicates perfect reflection. For the calculations, we assumed a typical value of C_D=2×10^{-3}, as in Henderson (2016).

For all the selected cases, $\mathcal{R} < 1$ and $D > 1$, illustrating some degree of vertical propagation occurred in all of them. The lowest values of $\mathcal{R}$ coincide with the highest values of D in systems where signatures of vertically propagating seiches were identified by Henderson (2016) (Frains Lake and Sau reservoir) and where the vertical propagation was reported (Lacamas Lake and La Fe reservoir). Lake Alpnach and Wood Lake are natural lakes with nearly flat bottom and alike rectangular morphometries, so they have the highest $\mathcal{R}$ and $D \sim 1$, with signatures of appreciable standing waves in the referred articles. The analysis supports that vertically propagating basin-scale internal waves is the rule rather than the exception.

Table 3. Parameters of internal wave reflection in selected lakes. [1] Münnich et al. (1992), [2] Lazerte (1980), [3] Serra et al. (2007), [4] Wiegand and Chamberlain (1987), [5] Henderson and Deemer (2012), [6] present study.

Lake [source]	L (m)	H (m)	N (Hz)	T (h)	v_{RMS} (m/s)	D	$\mathcal{R}$
Lake Alpnach [1]	5000	21.6	0.01	24	0.02	1.2	0.74
Frains Lake [2]	300	4	0.05	7	0.008	5.3	0.48
Sau reservoir [3]	3600	30	0.02	24	0.02	4.6	0.45
Wood Lake [4]	6800	26	0.02	24	0.02	2.1	0.80
Lacamas Lake [5]	1500	15	0.03	24	0.016	8.0	0.25†
La Fe reservoir [6]	1000	20	0.02	20	0.01	9.2	0.41†

†Directly estimated from the fit of a theoretical pattern to model or field results.

6. Conclusions

We used numerical modeling and theoretical inviscid wave ray tracing to explain observations of vertical gradual phase shifting of temperature oscillations in a steep reservoir. Due to the dominant supercritical reflection in the reservoir, 24-h period oscillations were identified as vertically propagating internal seiches, characterized by high coherence throughout the water column and gradual upward phase shifting of temperature and velocity

profiles, and standing waves of 24-h period did not form. For lower forcing frequencies, characteristic of higher order vertical modes, the supercritical reflection increases, so higher order vertical motions are more likely to occur as vertically propagating seiches and are less suitable to be described by standing mode theory.

We conclude that vertical propagating basin scale internal waves are ubiquitous to stratified lakes and reservoirs, due to the imperfect reflection of internal wave rays and viscous dissipation, whilst the non-dissipative modal description is a valid approximation in systems where subcritical reflection is significant, so the amount of upward propagating reflected energy is similar to the downward incident energy, despite some degree of vertical propagation always remains. The mechanisms described in this paper, which explain vertical propagation and standing mode preclusion, are expected to occur in any given lake, but their signatures are more evident in steep sided lakes, with a wide metalimnion and/or with a significant stratification extending through the water column. In some systems where significant supercritical reflection may be important, the modal description has been used with apparent success because the signature of vertically propagating waves is difficult to observe when there is a thin metalimnion separating well mixed epilimnion and hypolimnion.

7. Acknowledgments

The authors thank to Empresas Públicas de Medellín (EPM) for funding the field work and providing reservoir data.

8. Data availability statement

Software for this research is available in Hodges and Dallimore (2016) at https://www.hydronumerics.com.au/software/aquatic-ecosystem-model-3d. Configuration files for the simulations presented here and field data for this research will be available at a repository by the time of publication.

9. References

Boegman, L., J. Imberger, G. N. Ivey, and J. P. Antenucci. 2003. High-frequency internal waves in large stratified lakes. Limnol. Oceanogr. **48**: 895–919.

Cushman-Roisin, B., V. Tverberg, and E. G. Pavia. 1989. Resonance of internal waves in fjords: A finite-difference model. J. Mar. Res. **47**: 547–567. doi:10.1357/002224089785076190

Dauxois, T., A. Didier, and E. Falcon. 2004. Observation of near-critical reflection of internal waves in a stably stratified fluid. Phys. Fluids **16**: 1936–1941. doi:10.1063/1.1711814

Dissanayake, P., H. Hofmann, and F. Peeters. 2019. Comparison of results from two 3D hydrodynamic models with field data: internal seiches and horizontal currents. Inl. Waters **9**: 239–260. doi:10.1080/20442041.2019.1580079

Evans, M. A., S. MacIntyre, and G. W. Kling. 2008. Internal wave effects on photosynthesis: Experiments, theory, and modeling. Limnol. Oceanogr. **53**: 339–353. doi:10.4319/lo.2008.53.1.0339

Gill, A. E. 1982. Atmosphere-Ocean Dynamics, Academic Press.

Gómez-Giraldo, A., J. Imberger, and J. P. Antenucci. 2006. Spatial structure of the dominant basin-scale internal waves in Lake Kinneret. Limnol. Oceanogr. **51**: 229–246. doi:10.4319/lo.2006.51.1.0229

Gómez-Giraldo, A., J. Imberger, J. P. Antenucci, and P. S. Yeates. 2008. Wind-shear-generated high-frequency internal waves as precursors to mixing in a stratified lake. Limnol. Oceanogr. **53**: 354–367. doi:10.4319/lo.2008.53.1.0354

547 Grinsted, A., J. C. Moore, and S. Jevrejeva. 2004. Application of the cross wavelet transform
548 and wavelet coherence to geophysical time series. Nonlinear Process. Geophys. **11**:
549 561–566. doi:10.5194/npg-11-561-2004

550 Henderson, S. M. 2016. Turbulent production in an internal wave bottom boundary layer
551 maintained by a vertically propagating seiche. J. Geophys. Res. Ocean. **121**: 2481–2498.
552 doi:10.1002/2015JC011071

553 Henderson, S. M., and B. R. Deemer. 2012. Vertical propagation of lakewide internal waves.
554 Geophys. Res. Lett. **39**: n/a-n/a. doi:10.1029/2011GL050534

555 Hodges, B. R. 2000. Numerical Techniques in CWR-ELCOM (code release v. 1). CWR
556 Manuscr. WP **1422**.

557 Hodges, B. R., and C. Dallimore. 2013. Estuary, Lake and Coastal Ocean Model: ELCOM
558 v2. 2 science manual, Technical report, Centre for Water Research, Univ. of Western
559 Australia.

560 Hodges, B. R., and C. Dallimore. 2016. Aquatic Ecosystem Model: AEM3D, v1. 0. User
561 Manual, Hydronumerics, Aust. Melb.

562 Imam, Y. E., B. E. Laval, and G. a. Lawrence. 2013. The baroclinic response to wind in a
563 small two-basin lake. Aquat. Sci. **75**: 213–233. doi:10.1007/s00027-012-0268-1

564 Imberger, J. 1998. Flux paths in a stratified lake : A review, p. 1–17. *In* J. Imberger [ed.],
565 Physical Processes in lakes and oceans. Coastal and estuarine studies. V. 54. AGU.

566 Kocsis, O., B. Mathis, M. Gloor, M. Schurter, and A. Wüest. 1998. Enhanced mixing in
567 narrows: A case study at the Mainau sill (Lake Constance). Aquat. Sci. **60**: 236–252.

568 doi:10.1007/s000270050039

569 de la Fuente, A., K. Shimizu, J. Imberger, and Y. Niño. 2008. The evolution of internal waves
570 in a rotating, stratified, circular basin and the influence of weakly nonlinear and
571 nonhydrostatic accelerations. Limnol. Oceanogr. **53**: 2738–2748.
572 doi:10.4319/lo.2008.53.6.2738

573 de la Fuente, A., K. Shimizu, Y. Niño, and J. Imberger. 2010. Nonlinear and weakly
574 nonhydrostatic inviscid evolution of internal gravitational basin-scale waves in a large,
575 deep lake: Lake Constance. J. Geophys. Res. **115**: C12045. doi:10.1029/2009JC005839

576 Lazerte, B. D. 1980. The dominating higher order vertical modes of the internal seiche in a
577 small lake. Limnol. Oceanogr. **25**: 846–854. doi:10.4319/lo.1980.25.5.0846

578 Lemckert, C., J. Antenucci, A. Saggio, and J. Imberger. 2004. Physical Properties of
579 Turbulent Benthic Boundary Layers Generated by Internal Waves. J. Hydraul. Eng. **130**:
580 58–69. doi:10.1061/(ASCE)0733-9429(2004)130:1(58)

581 Maas, L. R. M., and F.-P. A. Lam. 1995. Geometric focusing of internal waves. J. Fluid
582 Mech. **300**: 1–41. doi:10.1017/S0022112095003582

583 Münnich, M., a. Wüest, and D. M. Imboden. 1992. Observations of the second vertical mode
584 of the internal seiche in an alpine lake. Limnol. Oceanogr. **37**: 1705–1719.
585 doi:10.4319/lo.1992.37.8.1705

586 Pernica, P., M. G. Wells, and W. G. Sprules. 2013. Internal waves and mixing in the
587 epilimnion of a lake affects spatial patterns of zooplankton in a body-size dependent
588 manner. Limnol. Oceanogr. Fluids Environ. **3**: 279–294. doi:10.1215/21573689-
589 2409149

590 Phillips, O. 1977. The Dynamics of the Upper Ocean, 2nd ed. Cambridge Univ Press.

591 Posada-Bedoya, A., A. Gómez-Giraldo, and R. Román-Botero. 2022. Decoupled basin-scale
592 internal waves in a continuously stratified two-basin tropical Andean reservoir.
593 Limnologica **93**: 125931. doi:10.1016/j.limno.2021.125931

594 Posada-Bedoya, A., A. Gómez-Giraldo, and R. Román Botero. 2019. Preliminary
595 characterization of the dominant baroclinic modes of a tropical Andean reservoir during
596 a dry period. Rev. la Acad. Colomb. Ciencias Exactas, Físicas y Nat. **43**: 297.
597 doi:10.18257/raccefyn.799

598 Posada-Bedoya, A., A. Gómez-Giraldo, and R. Román-Botero. 2021. Effects of riverine
599 inflows on the climatology of a tropical Andean reservoir. Limnol. Oceanogr.
600 lno.11897. doi:10.1002/lno.11897

601 Román-Botero, R., A. Gómez-Giraldo, and M. T. Botero. 2013. Efecto estacional de los
602 afluentes en la estructura térmica de un pequeño embalse neotropical, La Fe - Colombia.
603 Dyna **80**: 152–161.

604 Serra, T., J. Vidal, X. Casamitjana, M. Soler, and J. Colomer. 2007. The role of surface
605 vertical mixing in phytoplankton distribution in a stratified reservoir. Limnol. Oceanogr.
606 **52**: 620–634. doi:10.4319/lo.2007.52.2.0620

607 Shimizu, K., and J. Imberger. 2008. Energetics and damping of basin-scale internal waves in
608 a strongly stratified lake. Limnol. Oceanogr. **53**: 1574–1588.

609 Simpson, J. H., P. J. Wiles, and B. J. Lincoln. 2011. Internal seiche modes and bottom
610 boundary-layer dissipation in a temperate lake from acoustic measurements. Limnol.
611 Oceanogr. **56**: 1893–1906. doi:10.4319/lo.2011.56.5.1893

612 Sutherland, B. R. 2010. Internal Gravity Waves,.

613 Thorpe, S. a. 1998. Some dynamical effects of internal waves and the sloping sides of lakes.
614 Phys. Process. Lakes Ocean. Coast. Estuar. Stud. **54**: 441–460.

615 Turner, J. S. 1973. Buoyancy Effects in Fluids, Cambridge University Press.

616 Ulloa, H. N., K. B. Winters, A. de la Fuente, and Y. Niño. 2015. Degeneration of internal
617 Kelvin waves in a continuous two-layer stratification. J. Fluid Mech. **777**: 68–96.
618 doi:10.1017/jfm.2015.311

619 UNESCO. 1981. Tenth report of the joint panel on oceanographic tables and standards. Tech.
620 Pap. Mar. Sci. No. 36 24.

621 Vidal, J., and X. Casamitjana. 2008. Forced Resonant Oscillations as a Response to Periodic
622 Winds in a Stratified Reservoir. J. Hydraul. Eng. **134**: 416–425.
623 doi:10.1061/(ASCE)0733-9429(2008)134:4(416)

624 Vidal, J., S. MacIntyre, E. E. McPhee-Shaw, W. J. Shaw, and S. G. Monismith. 2013.
625 Temporal and spatial variability of the internal wave field in a lake with complex
626 morphometry. Limnol. Oceanogr. **58**: 1557–1580. doi:10.4319/lo.2013.58.5.1557

627 Wiegand, R. C., and V. Chamberlain. 1987. Internal waves of the second vertical mode in a
628 stratified lake. Limnol. Oceanogr. **32**: 29–42. doi:10.4319/lo.1987.32.1.0029

629 Woodward, B. L., C. L. Marti, J. Imberger, M. R. Hipsey, and C. E. Oldham. 2017. Wind
630 and buoyancy driven horizontal exchange in shallow embayments of a tropical
631 reservoir: Lake Argyle, Western Australia. Limnol. Oceanogr. **62**: 1636–1657.
632 doi:10.1002/lno.10522

633 Wüest, A., and A. Lorke. 2003. Small-Scale Hydrodynamics in Lakes. Annu. Rev. Fluid
634 Mech. **35**: 373–412. doi:10.1146/annurev.fluid.35.101101.161220

635